ACCSCIENCE PUBLISHING

Eurasian Journal of Medicine and Oncology

ORIGINAL RESEARCH ARTICLE

Super-enhancer gene *C1QTNF6* as a prognostic biomarker and therapeutic target in bladder cancer: A machine learning-based multi-omics analysis

Jun Chen[1†], Qingyuan Lin[2†], Honglin Zhu[1], and Xiaobing Li[1*]

[1]School of Health Science and Engineering, University of Shanghai for Science and Technology, Shanghai, China

[2]Department of Pathology, The Ninth People's Hospital, Shanghai Jiao Tong University School of Medicine, Shanghai, China

Abstract

Introduction: Super-enhancers play crucial roles in tumor development as key transcriptional regulatory elements, yet their prognostic value in bladder cancer (BLCA) remains to be systematically elucidated.

Objective: This study aimed to comprehensively analyze the regulatory mechanisms of super-enhancer-related genes (SERGs) in predicting BLCA prognosis and immune therapy response.

Methods: This study integrated BLCA RNA sequencing data from the cancer genome atlas (training set) and gene expression omnibus (validation set) databases and obtained SERG sets from the SEdb database. Using 101 machine learning ensemble frameworks, we screened and validated SERG sets with significant prognostic value and constructed a risk score model was constructed based on based on CoxBoost and plsRcox. Model performance was evaluated through nomograms. We conducted an in-depth analysis of the association between the risk model and tumor immune microenvironment, identified key hub genes through differential expression analysis, survival analysis, and receiver operating characteristic curve analysis, and performed multi-dimensional validation using immunohistochemistry and single-cell sequencing data.

Results: Through machine learning algorithm optimization, we identified eight core genes (*AHNAK*, *NT5DC3*, *NFIC*, *MTHFD1L*, *C1QTNF6*, *SLC45A3*, *QRICH2*, *KRT8*). High-risk group patients exhibited poor prognosis and elevated immune and tumor immune dysfunction and exclusion scores, suggesting potential immune therapy resistance. The single-sample gene set enrichment analysis analysis revealed significant positive correlations between risk scores and multiple key signaling pathways, including extracellular matrix-receptor interaction, regulation of actin cytoskeleton, and pathogenic *Escherichia coli* infection, focal adhesion, melanoma, and gap junction pathways. Further analysis indicated that *C1QTNF6* and *MTHFD1L* displayed significant potential as biomarkers based on expression profiles across cell types.

Conclusion: This study pioneered the construction of a prognostic prediction model for BLCA based on SERGs, revealing the crucial role of super-enhancers in regulating the tumor immune microenvironment and identifying potential therapeutic targets and prognostic markers. This research provides a new molecular typing strategy for the precision treatment of BLCA while establishing a theoretical foundation for personalized immunotherapy.

Keywords: Bladder cancer; Super-enhancer; Machine learning; Immune microenvironment; Single-cell RNA sequencing

[†]These authors contributed equally to this work

***Corresponding author:**
Xiaobing Li
(xiaobing@usst.edu.cn)

Citation: Chen J, Lin Q, Zhu H, Li X. Super-enhancer gene *C1QTNF6* as a prognostic biomarker and therapeutic target in bladder cancer: A machine learning-based multi-omics analysis. *Eurasian J Med Oncol*. 2025;9(4):191-208.
doi: 10.36922/EJMO025190171

Received: May 6, 2025

Revised: May 22, 2025

Accepted: May 27, 2025

Published online: June 20, 2025

1. Introduction

Bladder cancer (BLCA) ranks as the ninth-most common cancer globally, with approximately 614,000 new cases and 220,000 deaths in 2022.[1] Despite advances in diagnostic and therapeutic techniques, the 5-year survival rate for BLCA patients remains low, particularly for those with muscle-invasive BLCA.[2]

In recent years, understanding the molecular mechanisms underlying BLCA has become a critical research focus. Super-enhancers, as key epigenetic regulators, have emerged as pivotal elements in cancer development and progression. Our study specifically focuses on the *C1QTNF6* gene, which has garnered increasing attention in cancer research due to its potential regulatory roles in various tumor microenvironments (TMEs).

Prior studies have provided intriguing insights into the potential significance of *C1QTNF6* in cancer. For instance, Song *et al.*[3] demonstrated that *C1QTNF6* promotes oral squamous cell carcinoma. Zhang and Feng[4] found that *C1QTNF6* significantly promoted the proliferation of SPCA1 and A549 cells and remarkably reduced apoptosis. However, its specific role in BLCA remained largely unexplored, presenting a significant knowledge gap that our research aims to address.

Recent years have seen immunotherapy emerge as a promising treatment option for BLCA. For example, immune checkpoint inhibitors (ICIs) have demonstrated significant clinical efficacy in BLCA treatment.[5] However, not all patients benefit from immunotherapy, making the identification of effective predictive biomarkers crucial for guiding clinical treatment decisions.

Super-enhancers are cis-regulatory elements formed by clusters of conventional enhancers, characterized by unique epigenetic features and transcriptional regulatory functions.[6,7] They play crucial roles in maintaining cell identity and tumor development.[8] In various cancers, abnormal activation of super-enhancers is closely associated with oncogene upregulation.[9,10] Recent studies indicate that super-enhancers also participate in regulating the tumor immune microenvironment,[11] providing new perspectives for understanding tumor immune escape mechanisms.

Multiple studies have confirmed that super-enhancer abnormalities of specific genes are associated with tumor progression and prognosis.[12,13] In BLCA, SNHG15 and lncRNA LINC00162 have been reported to promote BLCA progression.[14,15] However, systematic analysis of the role of SERGs in the BLCA immune microenvironment and their prognostic value remain limited. A recent study found that expression patterns of certain SERGs may influence tumor immune infiltration and treatment response.[16] In addition, the development of single-cell sequencing technology has provided new tools for understanding the expression regulation of these genes across different cell types.[17,18]

Based on this background, our study aims to systematically evaluate the prognostic value of super-enhancer-related genes (SERGs) in BLCA, explore the specific molecular mechanisms of *C1QTNF6* in BLCA progression, investigate the potential of *C1QTNF6* as a diagnostic and therapeutic marker, and understand the role of *C1QTNF6* in the tumor immune microenvironment. By employing comprehensive bioinformatic analysis, including advanced machine learning approaches and multi-dimensional validation techniques, we seek to provide novel insights into BLCA's molecular landscape and potential personalized treatment strategies. Specifically, we hypothesize that *C1QTNF6*, as an important member of SERGs, may influence BLCA progression and drug sensitivity by regulating fibroblast function and epithelial cell interactions in the TME. This research has significant implications for discovering new prognostic markers and therapeutic targets, as well as optimizing patient prognosis prediction and treatment strategies.

2. Methods

2.1. BLCA data collection and processing

Gene expression profile data from BLCA patients were retrieved from the cancer genome atlas (TCGA) database (https://portal.gdc.cancer.gov/) and gene expression omnibus (GEO; https://www.ncbi.nlm.nih.gov/geo/). TCGA-BLCA served as the training set, while GSE13507 and GSE160693 were used as validation sets. To ensure comparability between datasets from different platforms (GSE13507 and GSE160693), batch effects were removed using the ComBat function from the R package "sva." The specific processing steps included: (i) identifying common genes; (ii) normalizing expression matrices; (iii) using the ComBat function with dataset identifiers as batch variables while considering biological covariates (such as tumor staging and grading); and (iv) validating the effect of batch effect removal through principal component analysis (PCA). This processing ensures the reliability and reproducibility of integrated analysis results across different datasets. SERGs were obtained from SEdb 2.0 (www.licpathway.net/sedb/).

2.2. Feature selection through 101 machine learning-based integration

Differential gene expression analysis of SERGs was performed using the R package "limma," with screening

criteria of log (fold change [FC]) = 1 and false discovery rate (FDR) < 0.05. Overlapping genes were obtained by taking the intersection of TCGA and GEO datasets, followed by univariate analysis. These overlapping genes were subjected to machine learning-based integration, incorporating 12 machine learning models, including partial least squares regression generalized linear model (plsRglm), extreme gradient boosting (XGBoost), Naive Bayes classifier (NaiveBayes), support vector machine (SVM), linear discriminant analysis (LDA), random forest (RF), least absolute shrinkage and selection operator (LASSO), Ridge regression (Ridge), gradient boosting machine (GBM), stepwise generalized linear model (Stepglm), elastic net (regularization) (Enet), and generalized linear model with component-wise boosting (glmBoost). We selected these 12 machine learning models based on their widespread application in cancer prognosis prediction and their unique algorithmic advantages: plsRglm provides the flexibility of partial least squares regression; XGBoost has advantages in handling high-dimensional data; NaiveBayes is suitable for scenarios with independent feature assumptions; SVM performs stably in high-dimensional feature spaces; LDA can effectively reduce dimensionality; RF improves generalization capability through random decision tree ensembles; LASSO and Ridge provide different forms of regularization to prevent overfitting; GBM enhances prediction accuracy through gradient boosting; Stepglm can perform stepwise feature selection; Enet combines the advantages of LASSO and Ridge; and glmBoost can handle variable selection in high-dimensional data. The combination of these models produced 101 algorithmic combinations, aiming to comprehensively evaluate the prognostic value of SERGs and determine the optimal prediction model. For the performance evaluation of each model, the concordance index (C-index) was calculated. The model with the highest average C-index score in both training and validation sets was considered optimal. Feature genes were then obtained through the best-performing model.

2.3. SERGs risk score and nomogram construction

We calculated individual risk scores for the obtained feature risk genes and divided patients in the training set into low- and high-risk groups using the median risk score as the threshold. Kaplan-Meier analysis was then applied to evaluate overall survival (OS) differences between these groups. In the BLCA patient test cohort, subgroup analyses were performed based on various clinicopathological features, including age, gender, pathological T stage, and tumor grade. Univariate and multivariate Cox regression analyses were conducted on clinical pathological indicators, including age, gender, pathological T stage, and tumor grade. A comprehensive multivariate regression model was then developed, combining risk scores with other independent prognostic factors to predict 1-, 3-, and 5-year OS rates. Using R packages "survcomp" and "rms," a nomogram was constructed to display the correlation between risk scores and clinicopathological features. The nomogram's predictive accuracy was evaluated through calibration plots, time-dependent receiver operating characteristic (ROC) curve analysis, C-index, and decision curve analysis.

2.4. SERGs risk score and immune-related analysis

The ESTIMATE algorithm and immune cell abundance identifier were employed to quantify immune infiltration scores and characterize tumor-infiltrating immune cells in BLCA samples. In addition, we performed a correlation analysis between risk scores and immune subgroups. We further established correlations between risk scores and immune checkpoints. By examining the relationship between risk scores and tumor immune dysfunction and exclusion (TIDE) scores (http://tide.dfci.harvard.edu/), we preliminarily assessed the risk score system's ability to predict patient response to immunotherapy.

2.5. SERGs risk score and tumor mutation correlation

To further investigate potential associations between SERG risk scores and tumor mutations, we conducted a detailed analysis of gene mutation differences between high- and low-risk groups. Specifically, we selected key genes associated with SERG risk scores and performed in-depth analysis combining mutation data from tumor samples. To ensure accuracy in data analysis and visualization, we comprehensively processed and displayed mutation data using the "maftools" package in R.

2.6. Risk score and single-sample gene set enrichment analysis (ssGSEA) correlation analysis

To explore potential associations between risk scores and biological pathways, this study utilized ssGSEA for quantitative pathway activity assessment and examined their correlation with risk scores. Specifically, the R packages "GSEABase" and "GSVA" were used to calculate enrichment scores for predefined gene sets to evaluate pathway activity levels in each sample. Subsequently, through Spearman correlation analysis, correlation coefficients (*R*-values) and significance levels (*p*-values) between risk scores and pathway enrichment scores were calculated to screen for biological pathways significantly correlated with risk scores.

2.7. Risk score and drug sensitivity analysis

While targeted drug therapy has made progress in BLCA treatment, the specific associations between SERG risk

models and drug sensitivity remain understudied. To address this research gap, this study aimed to explore the sensitivity of the SERGs-related risk model to potential target drugs in BLCA, screening for potentially effective therapeutic agents to provide a scientific basis for personalized treatment strategies. We utilized the R package "oncoPredict" for drug sensitivity analysis. This analysis predicts drug sensitivity indices based on the risk score model, combining gene expression and drug response data from public databases to evaluate potential patient responses to specific drugs.

2.8. Protein–protein interaction (PPI), expression, and prognosis of risk model genes

To comprehensively analyze the biological functions and clinical significance of risk model genes in BLCA, we employed a multi-angle analysis approach. Firstly, PPI networks were constructed through GeneMANIA (https://genemania.org/) to reveal potential interactions between risk model genes and their functional associations with other related proteins. Simultaneously, to clarify the expression characteristics of risk model genes in normal and tumor tissues, we conducted differential expression analysis (DEG) between normal and tumor groups, further combining paired sample data to analyze their expression patterns in individual samples. To further evaluate the predictive value of risk model genes for the prognosis of BLCA patients, we performed Kaplan Meier survival analysis on each SERG.

2.9. Hub gene ROC curves and immunohistochemical validation

To further screen key genes (hub genes) from SERGs, we conducted a systematic ROC curve analysis based on two independent BLCA datasets (GSE13507 and GSE52519). Specifically, the GSE13507 dataset was used as the test set for preliminary screening of hub genes with high diagnostic or predictive value, followed by validation analysis in the GSE52519 dataset to ensure the robustness and reproducibility of screening results. To further validate the actual expression levels of screened hub genes in BLCA tissues, we performed immunohistochemistry (IHC) experiments. IHC analysis was conducted on BLCA tissues and paired normal tissues, utilizing antibodies (Abcam, Britain) at a 1:500 dilution. Samples were fixed with 4% paraformaldehyde, embedded in paraffin, and sectioned (5-μm thickness). Phosphate-buffered saline was used instead of primary antibody as a negative control, and tissue known to express the target protein was used as a positive control. Each sample was repeated three times to ensure the reliability of the results.

2.10. Single-cell RNA (scRNA-seq) sequencing

scRNA-seq can reflect gene expression patterns with single-cell resolution, providing an important tool for studying gene-specific expression in different cell types and their microenvironment. To further explore the expression patterns of hub genes and their potential functions in BLCA, we performed single-cell sequencing analysis to reveal their expression characteristics across different cell subgroups. In this study, scRNA-seq technology was used to isolate single cells from BLCA patient samples for transcriptome sequencing. Data analysis followed a standardized processing pipeline, including quality control, removal of low-quality cells, gene expression normalization, dimensionality reduction clustering (t-distributed Stochastic Neighbor Embedding (t-SNE) or Uniform Manifold Approximation and Projection (UMAP)), and cell type annotation. ScRNA-seq was performed using the 10× Genomics Chromium platform. To reduce batch effects, all samples were processed in the same batch. Quality control criteria included: number of genes per cell >200 and <6000, UMI counts per cell >500 and <20000, and mitochondrial gene percentage <25%. The "Seurat" package was used for downstream analysis, including data normalization, identification of highly variable genes, PCA, cell clustering (resolution of 0.5), and DEG ($|\log FC| > 1$ and FDR < 0.05). Cell type annotation was based on published marker gene sets and validated through the "SingleR" package with reference datasets.

2.11. Molecular docking and hub gene expression

We utilized the "pRRophetic" package to predict the correlation between *C1QTNF6* expression levels and drug sensitivity. Based on *C1QTNF6* expression levels, samples were categorized into high-expression and low-expression groups. Molecular docking analysis was performed using the CB-Dock2 database[19] to evaluate the binding conformations between *C1QTNF6* and two compounds, Dasatinib and WH-4-02. In addition, BLCA tissue specimens were collected for histological evaluation by hematoxylin and eosin (H&E) staining, and *C1QTNF6* expression levels were assessed by IHC.

3. Results

3.1. Identification of SERGs and machine learning model development

Through preprocessing and DEG of TCGA-BLCA data, 84 SERGs were screened (Figure 1A). These genes displayed significant expression differences between tumor and normal tissues (Table S1), suggesting their potentially important roles in BLCA development and progression. To further analyze the key genes associated with patient

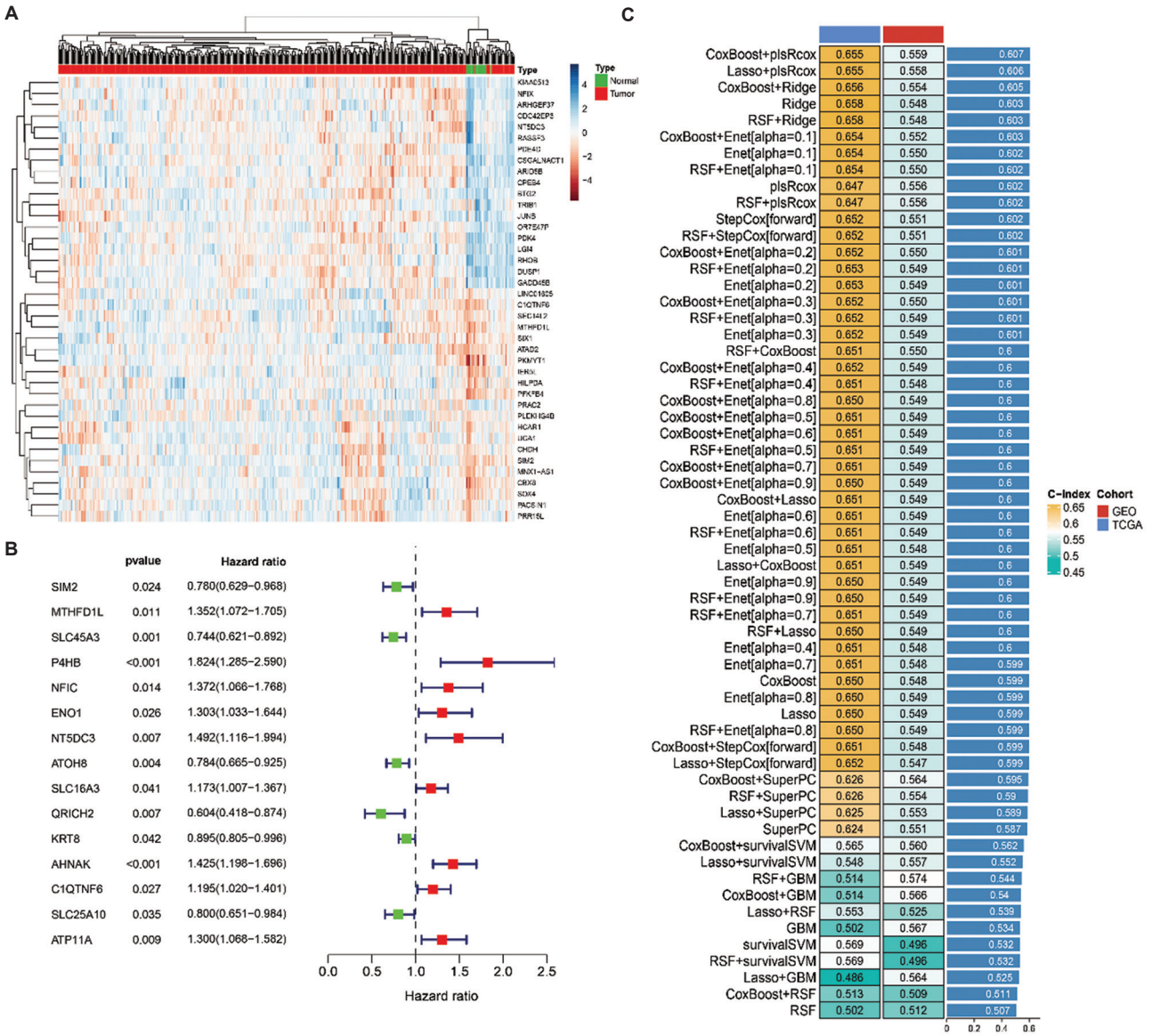

Figure 1. Identification and validation of super-enhancer-related gene (SERG) signatures. (A) Heatmap of the expression profiles of SERGs in normal and tumor groups; blue: Low expression, red: high expression. (B) Forest plot of the hazard ratios of SERGs. (C) Evaluation of survival prediction performance for SERGs using 101 machine learning models.

Table 1. Dasatinib free energy

CurPocket ID	Vina score (kcal/mol)	Cavity volume (Å^3)	Center (x, y, z)	Docking size (x, y, z)
C1	−5.5	150	−19, −1, −8	19, 19, 19
C2	−4.7	55	−15, 5, 15	19, 19, 19
C3	−4.7	53	−11, −3, −4	19, 19, 19
C4	−4.6	38	−11, 12, −1	19, 19, 19
C5	−4.1	40	2, 6, 6	19, 19, 19

prognosis, we used univariate Cox regression analysis to screen these 84 genes, ultimately identifying 15 SERGs with significant prognostic value (Figure 1B and Table 1). High or low expression of these genes was significantly associated with patients' OS, providing a basis for further modeling analysis. To construct an efficient risk prediction model, we used machine learning algorithms containing 101 combinations to evaluate these 15 prognosis-related SERGs. The final results indicate that the model based on CoxBoost and plsRcox combination performed best, with its C-index significantly higher than other models (Figure 1C), demonstrating excellent survival prediction capability.

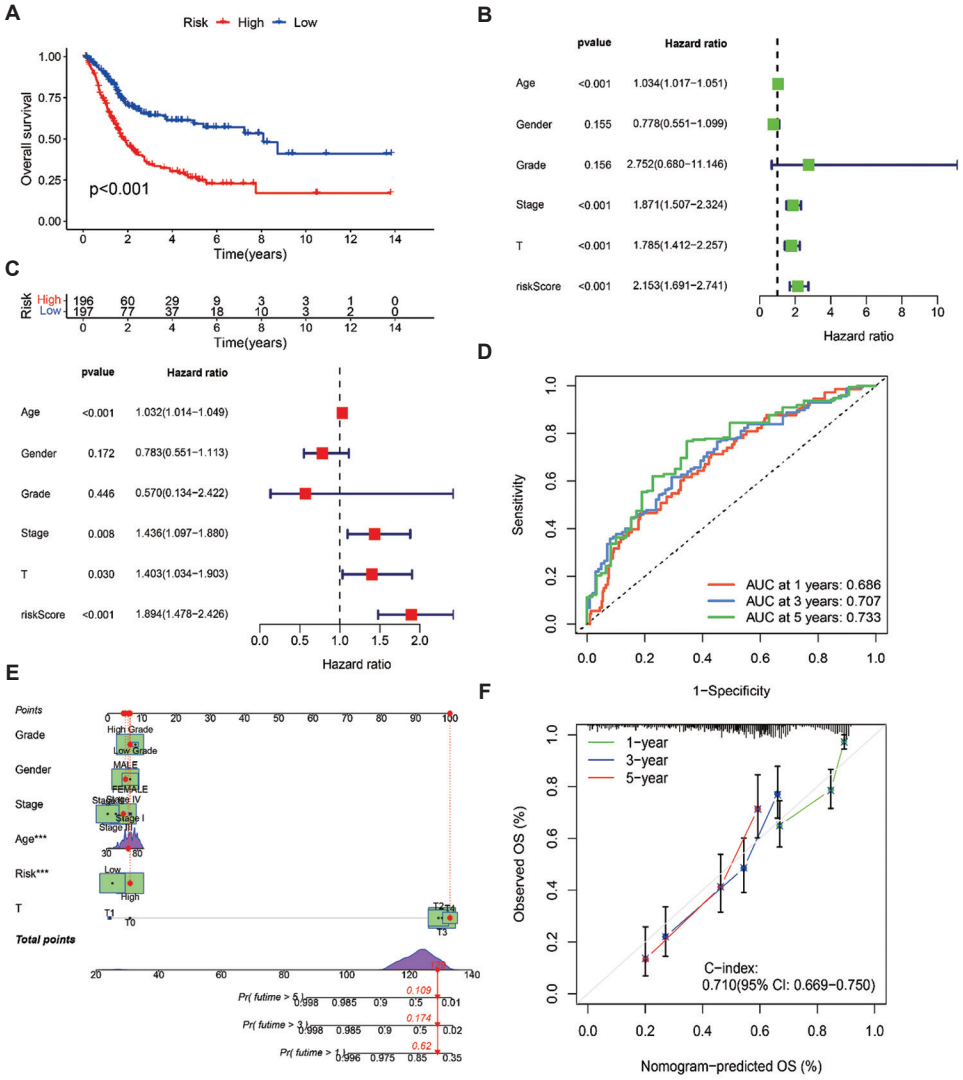

Figure 2. Survival analysis of super-enhancer-related gene risk score and nomogram construction. (A) Kaplan–Meier survival curves comparing overall survival (OS) between the high- and low-risk groups. (B and C) Univariate (B) and multivariate (C) Cox regression analyses displaying hazard ratios for multiple clinical features. (D) Receiver operating characteristic (ROC) curve assessing the accuracy of the risk score in predicting OS at 1-, 3-, and 5-year time points. (E) Nomogram combining multiple clinical variables and risk score to predict 1-, 3-, and 5-year survival probabilities. (F) Calibration curve evaluating the consistency between predicted survival probabilities (1, 3, and 5 years) from the nomogram and actual observed survival outcomes.

3.2. Risk score prognosis and nomogram construction

In the risk score and prognosis analysis, we found that risk scores could significantly differentiate the prognosis of BLCA patients. Kaplan–Meier survival analysis results indicated that high-risk patients had significantly shorter OS than low-risk patients, suggesting that risk score is a key factor affecting patient prognosis (Figure 2A). To further evaluate the independent prognostic value of risk scores and other clinicopathological features, we conducted univariate and multivariate Cox regression analyses in the training set. The results demonstrated that age, stage, pathological T stage, and risk score had independent prognostic significance (Figure 2B and C, Table 2), suggesting that these factors can independently predict patients' OS. Risk score demonstrated high hazard ratios

Table 2. WH-4-023 free energy

CurPocket ID	Vina score (kcal/mol)	Cavity volume (Å^3)	Center (x, y, z)	Docking size (x, y, z)
C1	−6.6	150	−19, −1, 8	25, 25, 25
C2	−6.5	55	−15, 5, 15	25, 25, 25
C3	−6.3	53	−11, −3, −4	25, 25, 25
C4	−6.0	38	−11,12, −1	25, 25, 25
C5	−5.6	40	2, 6, 6	25, 25, 25

(HR) (p<0.001; HR: 1.478 – 2.426). ROC curves reported high accuracy in predicting BLCA patient prognosis at 1, 3, and 5 years, with area under the curve (AUC) values reaching 0.686 (1-year), 0.707 (3-year), and 0.733 (5-year) (Figure 2D). These results indicate that the risk score model can accurately predict patients' short-term and long-term survival probabilities. Based on these results, we further constructed a nomogram model integrating risk scores with other independent prognostic factors (e.g., age, stage, pathological T stage) to quantify patient prognostic risk (Figure 2E). Calibration plot results demonstrated that the 1-, 3-, and 5-year calibration curves were close to the diagonal line, indicating good accuracy and consistency in the model's time-stratified predictions (Figure 2F).

3.3. Risk score correlation with immune microenvironment, immune function, and immunotherapy

To explore the relationship between risk scores and immunity, we conducted a comprehensive analysis. Results

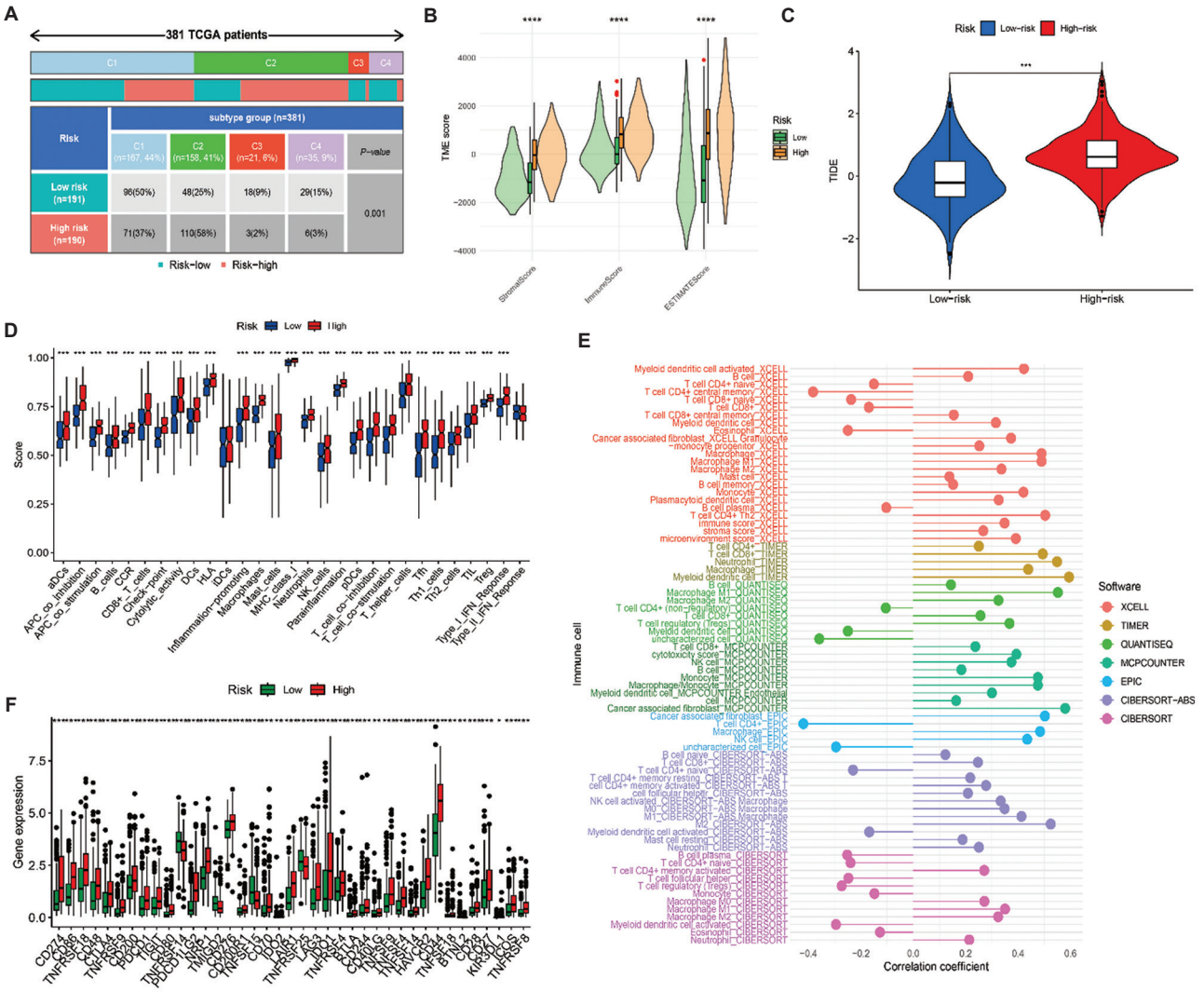

Figure 3. Association between super-enhancer-related gene risk score and immune characteristics in bladder cancer (BLCA). (A) Distribution of immune subtypes across high- and low-risk groups in 381 BLCA patients. Four distinct immune subtypes (C1 – C4) displayed significant association with risk stratification. (B) Comparison of tumor microenvironment scores between high- and low-risk groups. The high-risk group exhibited significantly elevated stromal score, immune score, and ESTIMATE score. (C) TIDE scores between risk groups; higher TIDE scores in the high-risk group indicate potential resistance to immune checkpoint inhibitor therapy. (D) Distribution of immune function scores across risk groups. Each axis represents a specific immune function, with the distance from the center indicating the enrichment score. The high-risk group demonstrated distinct immune function patterns compared to the low-risk group. (E) Correlation matrix displaying the relationship between risk score and various immune cell populations. (F) Differential expression of immune checkpoint genes between high- and low-risk groups. Notes: *p<0.05, **p<0.01, ***p<0.001, ****p<0.0001
Abbreviation: Tumor immune dysfunction and exclusion.

of immune subtype correlation with risk scores indicated that among the four immune subtypes C1, C2, C3, and C4, the proportion of C2 subtype patients in the high-risk group was significantly higher than other subtypes, while the C3 subtype was mainly concentrated in the low-risk group (p=0.001). These results suggest significant associations between different immune subtypes and patient risk scores (Figure 3A). Figure 3B presents differences in TME scores between high- and low-risk groups, including StromalScore, ImmuneScore, and ESTIMATE scores. The high-risk group displayed significantly higher scores in all three categories, suggesting that high-risk patients may have more complex TME characteristics, possibly accompanied by higher stromal components and immune cell infiltration. Elevated TIDE scores in the high-risk group suggest these patients may have higher immune evasion capability (Figure 3C). Correlation between risk scores and immune functions demonstrated that the high-risk group exhibited significantly enhanced activity in multiple functional modules, particularly in inflammation promotion, T-cell infiltration, and immune suppression modules (p<0.001), further indicating stronger immunosuppressive characteristics in the tumor immune microenvironment of high-risk patients (Figure 3D). Figure 3E reveals correlations between high-risk scores and various immune cell abundances, with the most significant positive correlations with myeloid cells (e.g., cancer-associated fibroblasts [CAF], myeloid dendritic cells [DC]) and certain T-cell subsets. This result was further validated using different computational methods (XCELL, TIMER, QUANTISEQ, etc.). Analysis of correlations between risk scores and immune checkpoint gene expression featured significantly elevated immune checkpoint gene expression in the high-risk group, suggesting the potential presence of an immunosuppressive microenvironment, providing a basis for potential ICI therapy (Figure 3F).

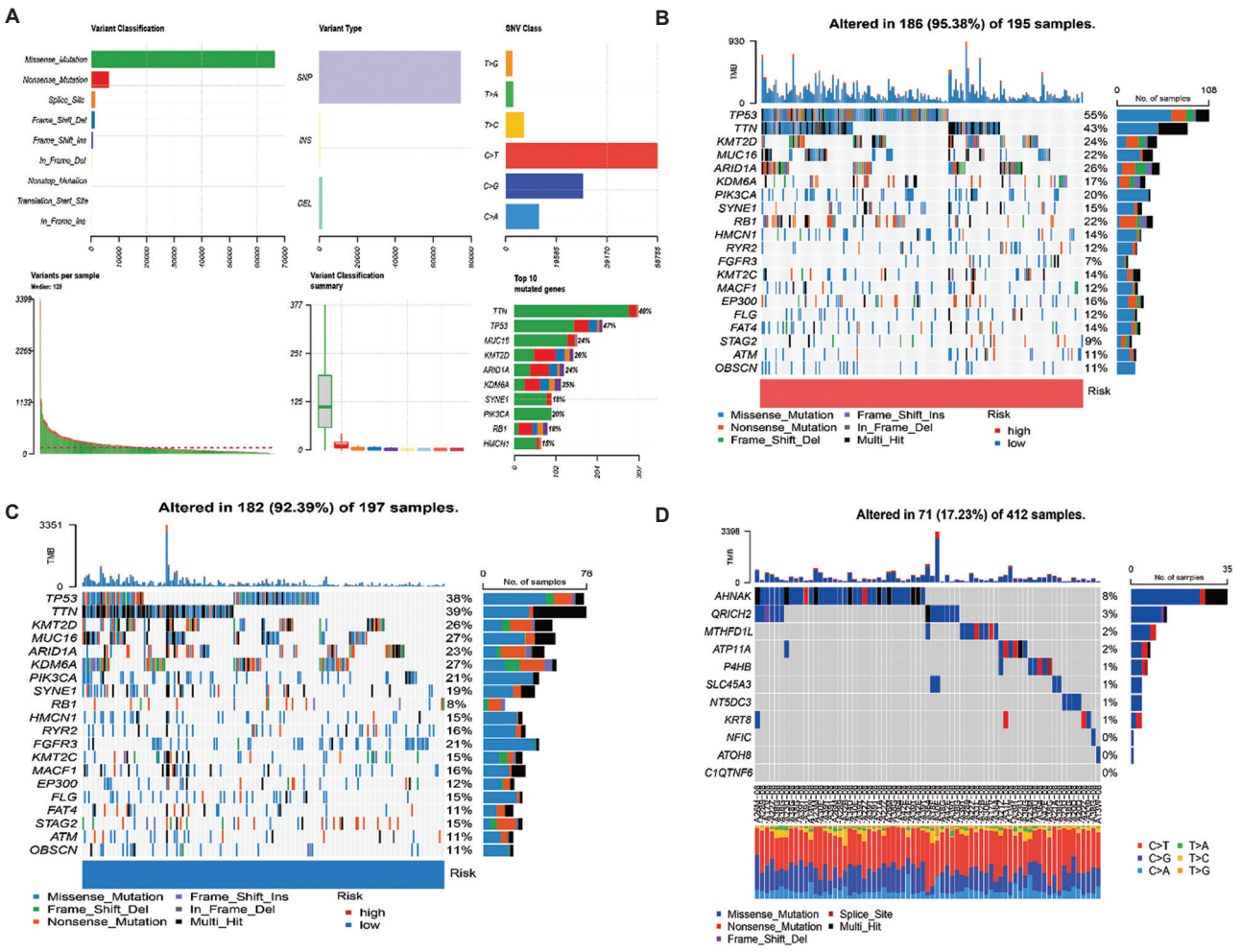

Figure 4. Mutational landscape associated with super-enhancer-related gene (SERG) risk score. (A) Overview of mutation types and frequencies in bladder cancer patients. (B) Mutation characteristics in the high-risk group. (C) Mutation patterns in the low-risk group. (D) Mutation profile of specific SERGs.

3.4. Risk score-related gene mutations

Figure 4A displays the classification and distribution characteristics of gene mutations in BLCA patients. Missense mutations were the predominant mutation type, accounting for the majority of total mutations. *TP53* was the most frequently mutated gene, with a mutation rate of 55% in the high-risk group, followed by *TTN* (43%) and *KMT2D* (24%) (Figure 4B). The low-risk group similarly expressed high-frequency mutations in *TP53* (38%) and *TTN* (39%) (Figure 4C). Among SERGs mutations, *AHNAK*, *QRICH2*, and *MTHFD1L* displayed relatively high mutation frequencies (Figure 4D).

3.5. Risk score and ssGSEA correlation

To further investigate the mechanisms by which risk scores affect BLCA, we performed ssGSEA analysis. Results indicated a significant positive correlation between risk scores and extracellular matrix (ECM)-receptor interaction pathway enrichment scores ($R = 0.63$; $p<2.2e-16$) (Figure 5A), suggesting that as risk scores increase, ECM-receptor interaction pathway activity significantly enhances. A strong positive correlation with the regulation of actin cytoskeleton ($R = 0.68$; $p<2.2e-16$) (Figure 5B) displayed significantly enhanced pathway activity in high-risk patients, possibly related to cell migration and tumor invasiveness. Figure 5C presents the significant positive correlation between risk scores and the pathogenic *Escherichia coli* infection pathway. In addition, risk scores exhibited positive correlations with focal adhesion, melanoma, and gap junction pathways (Figure 5D-F), possibly indicating significant associations with tumor progression.

3.6. SERG risk model gene expression and PPIs

Based on the optimal model combining CoxBoost and plsRcox, we obtained 11 risk model genes, including

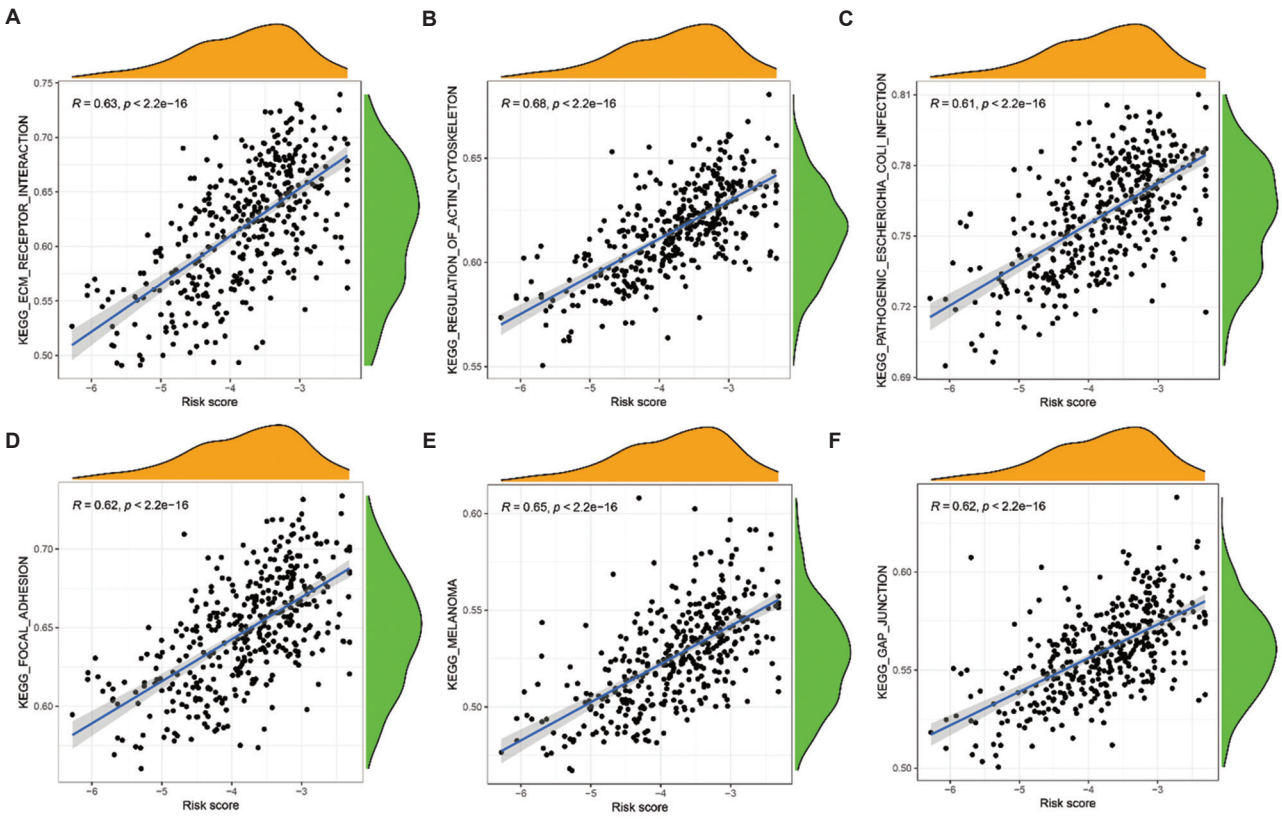

Figure 5. Correlation analysis between super-enhancer-related gene risk score and pathway enrichment based on single-sample gene set enrichment analysis. (A) Positive correlation between risk score and extracellular matrix (ECM)-receptor interaction pathway ($R = 0.63$; $p<2.2e-16$). (B) Correlation analysis of risk score with regulation of actin cytoskeleton pathway ($R = 0.68$; $p<2.2e-16$), indicating a strong association between risk score and cytoskeletal organization. (C) Relationship between risk score and pathogenic *Escherichia coli* infection pathway enrichment scores. The positive correlation suggests the potential involvement of inflammatory responses in high-risk patients. (D) Analysis displaying a positive correlation between risk score and focal adhesion pathway enrichment scores. Enhanced focal adhesion signaling in high-risk patients may contribute to increased tumor cell adhesion and migration capabilities. (E) Correlation plot demonstrating the association between risk score and melanoma pathway activation, suggesting shared oncogenic mechanisms between bladder cancer and melanoma progression. (F) Positive correlation between risk score and gap junction pathway activity.

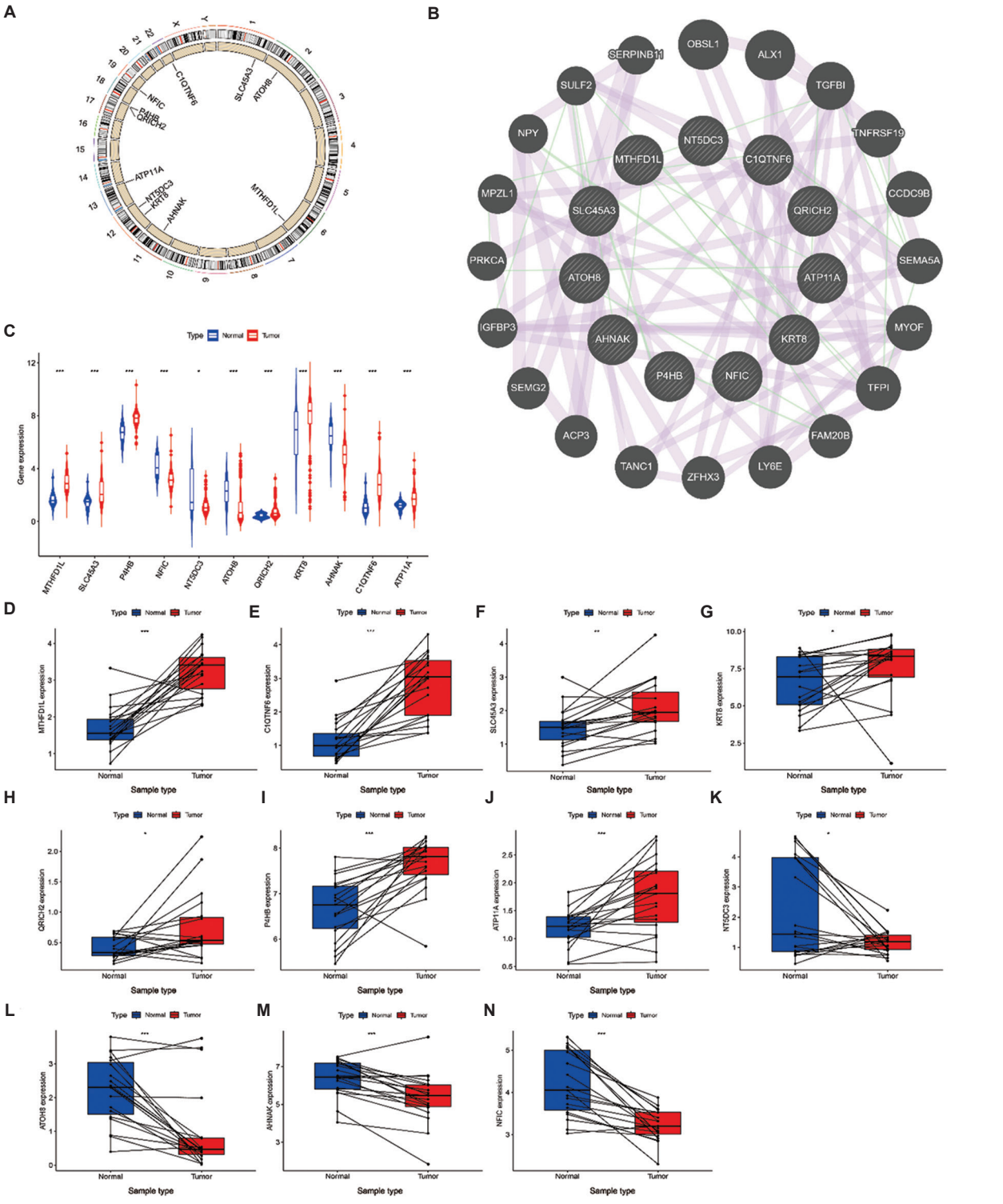

Figure 6. Expression of super-enhancer-associated hub genes. (A) Chromosomal distribution of super-enhancer-associated hub genes. (B) Protein-protein interaction network of super-enhancer-associated hub genes. (C) Differential expression of super-enhancer-associated hub genes between normal and tumor tissues. (D-J) Expression of hub genes in paired tumor and normal tissues displays an upregulation of *MTHFD1L* (D), *C1QTNF6* (E), *SLC45A3* (F), *KRT8* (G), *QRICH2* (H), *P4HB* (I), and *ATP11A* (J). (K-N) A downregulation of *NT5DC3* (K), *ATOH8* (L), *AHNAK* (M), and *NFIC* (N) is observed. Notes: *p<0.05, **p<0.01, ***p<0.001

MTHFD1L, *SLC45A3*, *P4HB*, *NFIC*, *NT5DC3*, *ATOH8*, *QRICH2*, *KRT8*, *AHNAK*, *C1QTNF6*, and *ATP11A*. Figure 6A displays the chromosomal location distribution of SERGs. *C1QTNF6* is located on chromosome 1, *MTHFD1L* on chromosome 6, *AHNAK* and *NFIC* on chromosome 11, and *ATP11A* on chromosome 13, among others. Through the PPI network construction of SERGs and their interactions, core genes, such as *C1QTNF6*, *MTHFD1L*, *NFIC*, *KRT8*, and *AHNAK*, formed significant interaction networks with multiple proteins (Figure 6B). Furthermore, differential expression of SERGs between normal and tumor tissues revealed that *C1QTNF6*, *MTHFD1L*, *SLC45A3*, *AHNAK*, and *P4HB* were significantly upregulated in tumor tissues, while other genes (*NFIC* and *QRICH2*) were downregulated in tumors (Figure 6C). Expression of SERGs in paired tumor and normal tissues displayed an upregulation of *MTHFD1L*, *C1QTNF6*, *SLC45A3*, *KRT8*, *QRICH2*, *P4HB*, and *ATP11A* (Figure 6D-J), while *NT5DC3*, *ATOH8*, *AHNAK*, and *NFIC* displayed a downregulation (Figure 6K-N). Paired analysis indicates consistent expression patterns of SERGs in tumor tissues, further supporting their clinical significance as potential biomarkers.

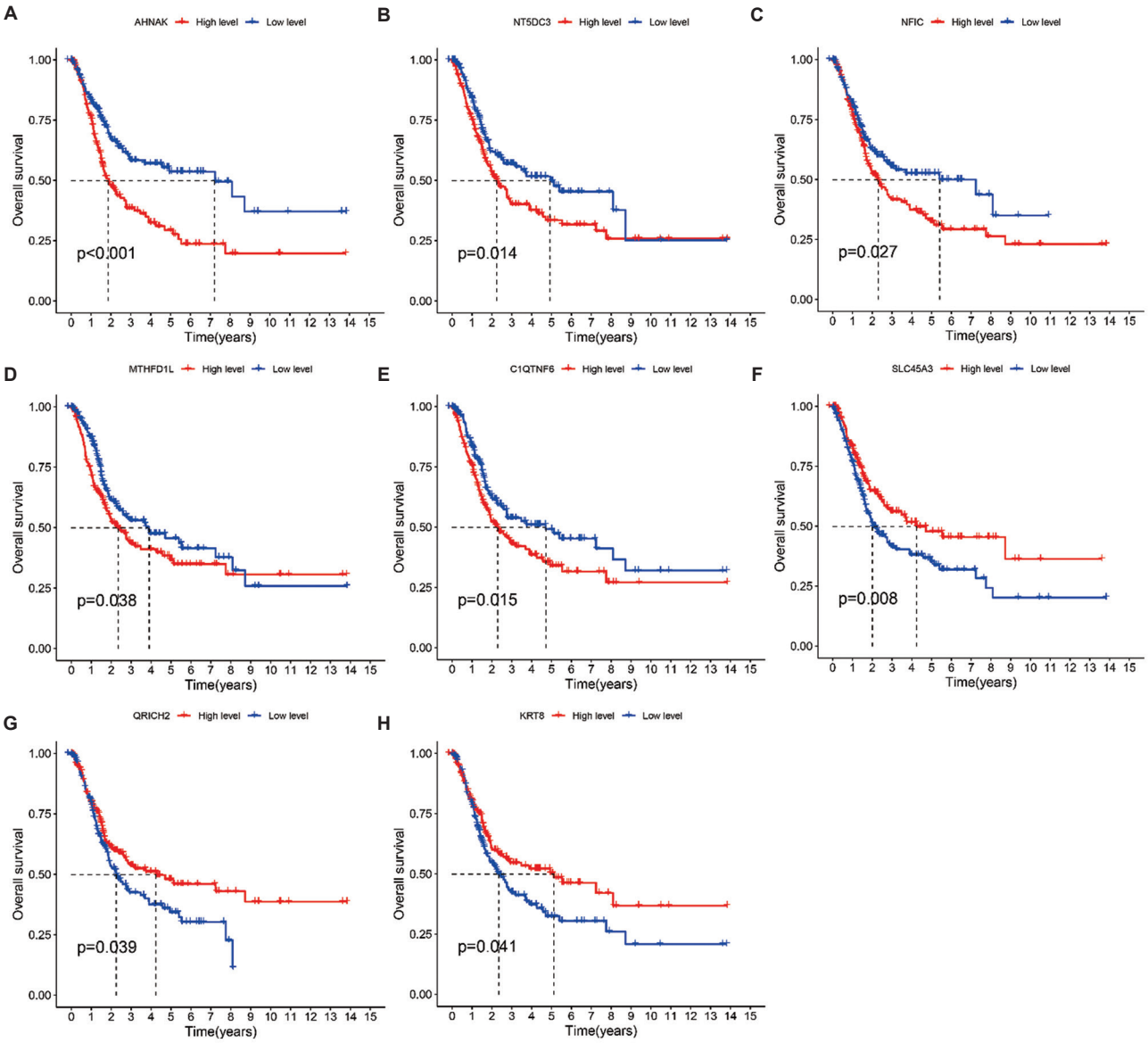

Figure 7. Correlation between hub gene expression levels and overall survival. (A-E) High expression of *AHNAK* (A), *NT5DC3* (B), *NFIC* (C), *MTHFD1L* (D), and *C1QTNF6* (E) correlates with poor survival in patients with bladder cancer (BLCA). (F-H) Low expression of *SLC45A3* (F), *QRICH2* (G), and *KRT8* (H) correlates with poor survival in patients with BLCA.

3.7. SERG risk model gene prognosis and hub gene selection

Prognostic analysis of SERG risk model genes revealed significant associations between multiple genes and BLCA patient survival outcomes. Specifically, high expression of *AHNAK*, *NT5DC3*, *NFIC*, *MTHFD1L*, and *C1QTNF6* was closely associated with poor patient prognosis, suggesting these genes may promote malignant tumor progression (Figure 7A-E). In contrast, high expression of *SLC45A3*, *QRICH2*, and *KRT8* was associated with longer survival periods, suggesting potential protective roles in tumors (Figure 7F-H). Based on expression characteristics of SERG risk model genes and their associations with prognosis, *C1QTNF6* and *MTHFD1L* were prioritized as key candidate genes and validated in independent external datasets. We selected the GSE13507 dataset as the test set and the GSE52519 dataset as the validation set, evaluating the diagnostic performance of these two genes through ROC curves. In the GSE13507 test set, *C1QTNF6* and *MTHFD1L* reported AUC values of 0.815 and 1.000, respectively (Figure 8A and B), demonstrating excellent diagnostic performance. In the GSE52519 validation set, *C1QTNF6* and *MTHFD1L* reported AUC values of 0.72 and 0.684, respectively (Figure 8C and D), further validating their robustness and reliability across different datasets. The combined results from prognostic analysis, risk modeling, and external validation data suggested that *C1QTNF6* has the most prominent performance in diagnostic efficiency and prognostic correlation. Therefore, we selected *C1QTNF6* as the core gene for subsequent research, providing the basis for exploring its molecular mechanisms and clinical application value in BLCA.

3.8. Analysis of *C1QTNF6* gene expression patterns in different BLCA cell types

To further validate *C1QTNF6* expression in BLCA, we focused on studying its expression patterns at the single-

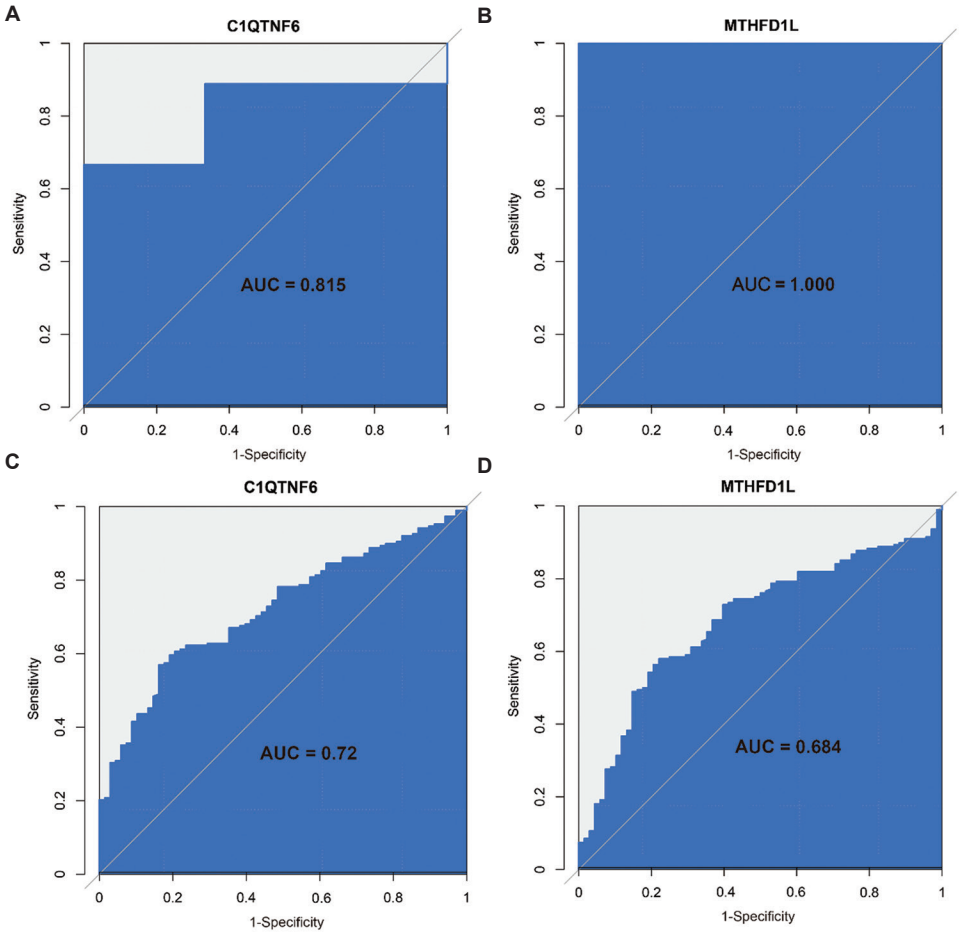

Figure 8. Receiver operating characteristic (ROC) curve analysis of hub genes. (A and B) ROC curve analysis demonstrating the diagnostic performance of *C1QTNF6* (A) and *MTHFD1L* (B) genes in the training cohort. (C and D) Validation of diagnostic efficacy through ROC curve analysis of *C1QTNF6* (C) and *MTHFD1L* (D) genes in the independent validation cohort.
Abbreviation: AUC: Area under the curve.

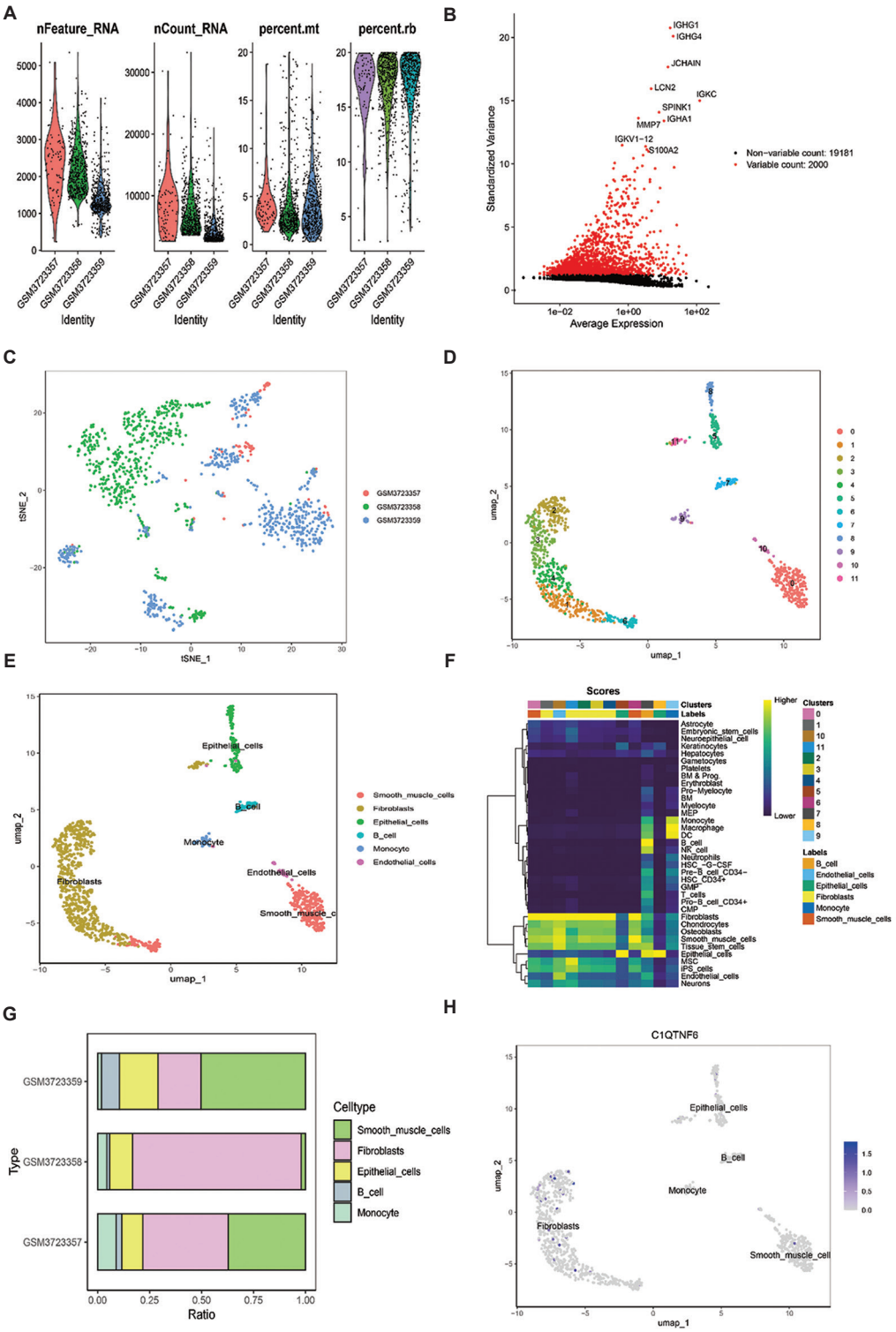

Figure 9. Single-cell RNA sequencing analysis and *C1QTNF6* expression across different cell types. (A) Quality control metrics across samples displaying the distribution of "nFeature_RNA," "nCount_RNA," "percent.mt," and "percent.rb." (B) Analysis of gene expression variability. (C) Sample distribution based on the t-SNE dimensionality reduction plot. (D) Cell clustering based on the UMAP dimensionality reduction plot. (E) UMAP visualization of cell type distribution, including smooth muscle cells, fibroblasts, epithelial cells, B cells, monocytes, and endothelial cells. (F) Expression heatmap of cell subpopulations depicting smooth muscle cells, fibroblasts, B cells, monocytes, and endothelial cells. (G) Proportion distribution of cell types across different samples. (H) Expression distribution of *C1QTNF6* across different cell types.

cell level. Figure 9A displays quality control metrics for single-cell sequencing samples, including "nFeature_RNA," "nCount_RNA," "percent.mt," and "percent.rb." We also screened the top 2000 highly variable genes (Figure 9B). Through t-SNE and UMAP dimensionality reduction clustering, all cells were divided into 12 clusters (Figure 9C and D). Through marker gene expression analysis, cell populations were classified into specific cell types, including smooth muscle cells, fibroblasts, epithelial cells, monocytes, B-cells, and endothelial cells (Figure 9E). Cell subgroup correlation with six specific cell expressions revealed that DC was significantly correlated with monocytes, while epithelial cells were significantly correlated with B-cells (Figure 9F). In the proportion distribution of different cell types across three samples, smooth muscle cells and fibroblasts expressed the highest proportions, suggesting the TME may be dominated by these cell types (Figure 9G). In addition, hub gene *C1QTNF6* expressed the highest expression levels in fibroblasts, followed by epithelial cells and monocytes, while its expression was relatively low in smooth muscle cells. This specific expression pattern suggests that *C1QTNF6* may play important roles in the TME by regulating fibroblast and epithelial cell functions (Figure 9H). The combined results with functional enrichment analysis indicated a significant association between *C1QTNF6* and both ECM remodeling and cell adhesion-related pathways ($p<0.001$). Furthermore, recent research by Huang and Qi[20] confirmed that *C1QTNF6* plays a key role in regulating angiogenesis in head and neck squamous cell carcinoma. Liu *et al.*[21] also reported that *C1QTNF6* was mainly expressed in fibroblasts; *in vitro* experiments validated silencing *C1QTNF6* in fibroblasts could inhibit M2 macrophage polarization and migration, further supporting our finding that C1QTNF6 may participate in TME regulation by affecting fibroblast function.

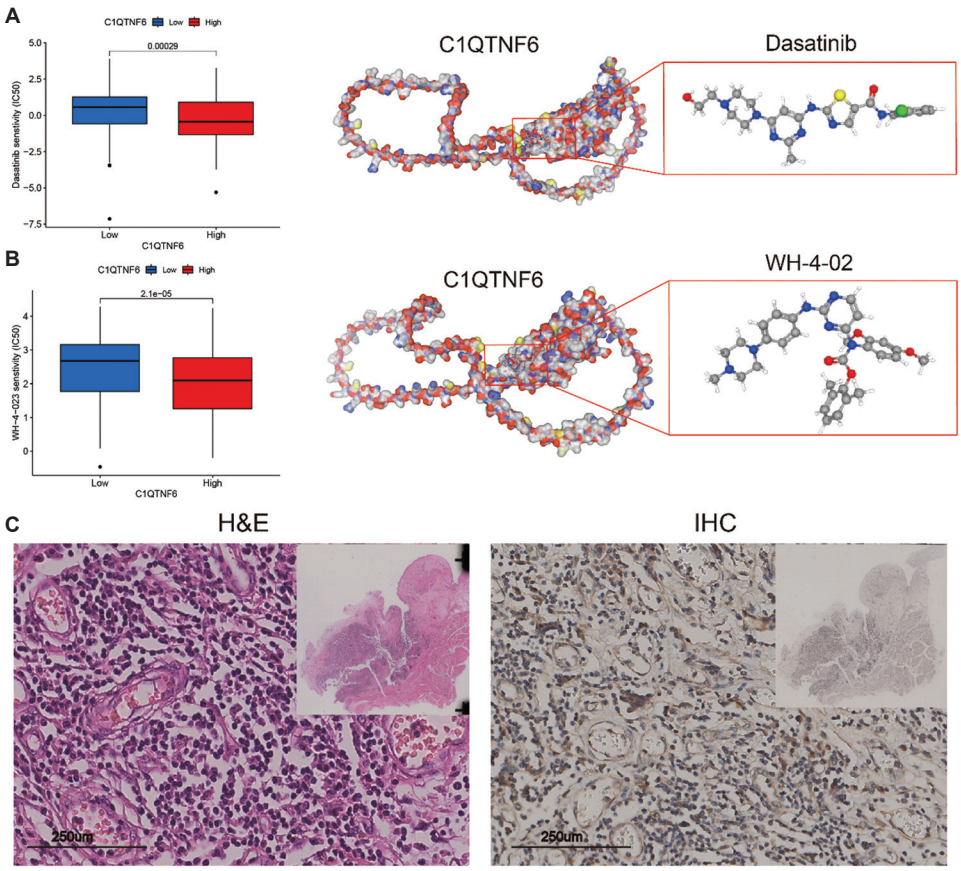

Figure 10. Comprehensive analysis of *C1QTNF6* in bladder cancer. (A) The high-expression group (red) displays markedly different sensitivity compared to the low-expression group (blue). Molecular docking visualization illustrates the structural interaction between C1QTNF6 and Dasatinib. (B) Notable difference in drug sensitivity between low- (blue) and high- (red) expression groups. Molecular docking representation features the binding configuration of C1QTNF6 with WH-4-02. (C) Hematoxylin and eosin (H&E) staining reveals dense cellular infiltration and altered tissue architecture. Immunohistochemistry (IHC) staining confirms the high expression of C1QTNF6 in bladder cancer tissues. Magnification: 20×; Scale bar: 250 μm.

3.9. Molecular docking and C1QTNF6 expression

Drug sensitivity analysis demonstrated that the high *C1QTNF6* expression group exhibited significantly greater sensitivity to Dasatinib compared to the low-expression group (p=0.00029), indicating that elevated *C1QTNF6* expression may enhance responsiveness to Dasatinib treatment (Figure 10A). Similarly, sensitivity to WH-4-02 was significantly enhanced in the high *C1QTNF6* expression group (p=2.1e-05) (Figure 10B). The Dasatinib and WH-4-023 free energies are displayed in Tables 1 and 2, respectively. Molecular docking results illustrated the binding conformations between the C1QTNF6 protein and both compounds, revealing favorable binding interactions between the two drugs and C1QTNF6. For Dasatinib, the most thermodynamically stable binding structure had a Vina score of −5.5 kcal/mol in cavity C1 (volume: 150 Å^3), indicating strong binding affinity. Similarly, WH-4-023 demonstrated even stronger binding with a Vina score of −6.6 kcal/mol in the same cavity, suggesting potentially higher therapeutic efficacy. These negative binding scores indicate thermodynamically favorable interactions, supporting the potential of both compounds as therapeutic agents targeting C1QTNF6. The binding occurs in the largest cavity (150 Å^3), which typically represents the most druggable site on the protein, further supporting the clinical relevance of these interactions. H&E staining demonstrated typical pathological features of BLCA tissue, characterized by abnormal cellular morphology and disorganized arrangement. IHC staining confirmed high expression of C1QTNF6 in BLCA tissues (Figure 10C). These findings suggest that *C1QTNF6* may serve as a potential therapeutic marker for drug treatment in BLCA.

4. Discussion

BLCA is one of the most common urological malignancies and among the most prevalent cancers globally.[22] In recent years, with a deeper understanding of epigenetics, super-enhancers, as key transcriptional regulatory elements, have received increasing attention for their roles in tumor development and progression.[23] This study systematically analyzed the expression characteristics and clinical significance of SERGs in BLCA, not only deepening our understanding of BLCA pathogenesis mechanisms but also providing new insights for clinical precision therapy.

First, this study discovered unique expression profiles of SERGs in BLCA tissue through integrated analysis. Previous studies have demonstrated that super-enhancers can influence tumor development by regulating key transcription factor expression. For example, in colorectal cancer, MYC-associated super-enhancer abnormal activation is closely related to tumor progression.[24] In liver cancer, super-enhancers maintain cancer stem cell properties by regulating SOX9 expression.[12] Our study is the first to systematically map the expression profile of SERGs in BLCA, identifying significant changes in the expression of multiple genes, including *AHNAK*, *NT5DC3*, and *NFIC*. The abnormal expression of these genes may participate in BLCA progression by affecting cell proliferation, apoptosis, and metastasis.[7]

More importantly, the prognostic prediction model established through machine learning methods not only demonstrates good predictive performance but also reveals the key role of super-enhancers in regulating the tumor immune microenvironment. Recent studies have demonstrated that epigenetic regulation plays an important role in shaping the tumor immune microenvironment.[25,26] Our study found that high-risk scores are associated with stronger immunosuppressive characteristics. Notably, high-risk group patients exhibited higher TIDE scores, suggesting potential immunotherapy resistance. This finding has important implications for guiding the personalized application of immunotherapy.

This study revealed the cell-specific expression pattern of *C1QTNF6* in the TME through single-cell sequencing technology. Previous studies mainly focused on the role of super-enhancers in tumor cells while overlooking their regulatory functions in the microenvironment. We found that *C1QTNF6* is highly expressed in fibroblasts, providing a new perspective for understanding tumor-stroma interactions. CAFs, as crucial components of the TME, influence tumor progression by secreting cytokines and remodeling the ECM.[27] High expression of *C1QTNF6* may affect various processes such as ECM remodeling and immune cell recruitment by regulating CAF activation states.[28,29] Multiple studies have demonstrated that *C1QTNF6* expression is associated with various tumors; for instance, *C1QTNF6* can influence lung cancer progression.[30] Huang and Qi[20] demonstrated that *C1QTNF6* inhibits angiogenesis in head-and-neck squamous cell carcinoma.

More critically, our study revealed the potential clinical value of *C1QTNF6* in BLCA therapy. Drug sensitivity analysis demonstrated that the high-expression group of C1QTNF6 exhibited significantly enhanced sensitivity to Dasatinib and WH-4-02 compared to the low-expression group. Molecular docking results further substantiated the favorable binding interaction between the C1QTNF6 protein and these two drugs. IHC staining confirmed the elevated expression of *C1QTNF6* in BLCA tissues. These findings not only substantiate the potential of *C1QTNF6* as a promising pharmacotherapeutic biomarker but also provide a novel theoretical foundation for personalized treatment strategies.

Furthermore, ssGSEA analysis revealed significant correlations between risk scores and multiple signaling pathways, including ECM-receptor interaction. This result corroborates recent findings that super-enhancers can promote tumor progression through coordinated regulation of multiple downstream effector molecules.[13,31] In particular, activation of the ECM-receptor interaction pathway not only affects tumor cell invasion and metastasis but may also influence treatment response by remodeling the immune microenvironment.[32]

From a clinical application perspective, this study has significant translational value. First, the prediction model based on SERGs can serve as an important tool for clinical stratified treatment. Second, the in-depth understanding of immune microenvironment characteristics provides new insights for optimizing immunotherapy. For example, high-risk patients may need to consider combination therapy strategies targeting the TME.[33] In addition, the discovery of key targets such as *C1QTNF6* provides direction for developing new therapeutic targets.

This study revealed the cell-specific expression pattern of *C1QTNF6* in the TME through single-cell sequencing technology. Notably, *C1QTNF6* demonstrates important roles in various cancers. Cai *et al.*[30] demonstrated that *C1QTNF6* protects lung cancer cells from ferroptosis by destabilizing *SOCS2* and enhancing the xCT/GPX4 pathway, thereby promoting lung cancer progression and metastasis. Qu *et al.*[34] demonstrated that *C1QTNF6* serves an important role in the development of gastric carcinoma, promoting proliferation and migration and reducing apoptosis of gastric carcinoma cells. In addition, Dong *et al.*[35] reported that CTRP6 inhibits PDGF-BB-induced vascular smooth muscle cells proliferation and migration by suppressing the PI3K/Akt/mTOR signaling pathway. These studies complement our findings in BLCA, collectively revealing the broad mechanism of *C1QTNF6* as a potential tumor promoter.

However, this study has several limitations. First, although we predicted multiple potential mechanisms through bioinformatics methods, these mechanisms still require experimental validation. Second, the clinical application value of the model requires further validation through prospective studies. Finally, the detailed mechanisms of how super-enhancers coordinately regulate multiple downstream genes warrant in-depth investigation.

As aforementioned, this study has significant clinical translational value. However, we believe future research should focus on the following directions: (i) designing *in vivo* experiments to validate the function of *C1QTNF6* in BLCA progression, such as constructing *C1QTNF6*-knockout/overexpressed BLCA cell lines and establishing nude mouse subcutaneous xenograft models; (ii) exploring the molecular mechanism of *C1QTNF6*'s association with Dasatinib sensitivity through *in vitro* cell experiments, comparing IC50 value differences between cells with high- and low-C1QTNF6 expression and analyzing changes in downstream key signaling pathways; (iii) conducting prospective clinical studies to validate the relationship between *C1QTNF6* expression levels and immunotherapy response, especially by analyzing the correlation between *C1QTNF6* expression and clinical response from biopsy samples collected from patients receiving ICI treatment; (iv) further elucidating how super-enhancers coordinately regulate multiple downstream genes through chromatin immunoprecipitation sequencing (ChIP-seq) and chromatin conformation capture technique (Hi-C) to identify super-enhancer regions and their regulatory factors associated with *C1QTNF6*. These studies will help deepen the understanding of BLCA pathogenesis and provide new strategies for precision clinical treatment.

5. Conclusion

Through multi-omics integrative analysis, this study comprehensively elucidates the critical regulatory role of SERGs in BLCA initiation and progression for the 1st time. By leveraging machine learning methodologies, we constructed a prognostic prediction model based on SERGs. This model not only achieved accurate patient outcome predictions but, more importantly, unveiled the pivotal role of super-enhancers in modulating the tumor immune microenvironment. Notably, we first identified and validated the elevated expression of *C1QTNF6* in BLCA tissues, along with its specific high expression in fibroblasts and potential regulatory mechanisms. Preliminary drug sensitivity analysis suggests that *C1QTNF6* expression levels are associated with sensitivity to dasatinib and WH-4-02, indicating its potential as a reference indicator for BLCA treatment strategy selection in the future. However, our findings warrant further validation through prospective clinical studies and mechanistic experiments. This research provides important insights for understanding BLCA pathogenesis and developing innovative therapeutic strategies.

Acknowledgments

None.

Funding

None.

Conflict of interest

The authors declare that they have no conflict of interest.

Author contributions

Conceptualization: Xiaobing Li
Formal analysis: All authors
Investigation: Xiaobing Li, Qingyuan Lin, Honglin Zhu
Writing – original draft: Jun Chen
Writing – review & editing: Jun Chen, Xiaobing Li

Ethics approval and consent to participate

Not applicable.

Consent for publication

Not applicable.

Availability of data

The data are available in the following public repositories: The Cancer Genome Atlas (TCGA) database (https://portal.gdc.cancer.gov/) and Gene Expression Omnibus (GEO; https://www.ncbi.nlm.nih.gov/geo/).

References

1. Bray F, Laversanne M, Sung H, *et al.* Global cancer statistics 2022: Globocan estimates of incidence and mortality worldwide for 36 cancers in 185 countries. *CA Cancer J Clin*. 2024;74(3):229-263.

   doi: 10.3322/caac.21834

2. Gontero P, Birtle A, Capoun O, *et al.* European association of urology guidelines on non-muscle-invasive bladder cancer (tat1 and carcinoma *in situ*)-a summary of the 2024 guidelines update. *Eur Urol*. 2024;86:531-549.

   doi: 10.1016/j.eururo.2024.07.027.

3. Song X, Li L, Shi L, *et al.* C1QTNF6 promotes oral squamous cell carcinoma by enhancing proliferation and inhibiting apoptosis. *Cancer Cell Int*. 2021;21(1):666.

   doi: 10.1186/s12935-021-02377-x

4. Zhang W, Feng G. C1QTNF6 regulates cell proliferation and apoptosis of NSCLC *in vitro* and *in vivo*. *Biosci Rep*. 2021;41(1).

   doi: 10.1042/bsr20201541

5. Sharma P, Siefker-Radtke A, De Braud F, *et al.* Nivolumab Alone and With ipilimumab in previously treated metastatic urothelial carcinoma: CheckMate 032 nivolumab 1 mg/kg plus ipilimumab 3 mg/kg expansion cohort results. *J Clin Oncol*. 2019;37:1608-1616.

   doi: 10.1200/jco.19.00538

6. Hnisz D, Abraham BJ, Lee TI, *et al.* Super-enhancers in the control of cell identity and disease. *Cell*. 2013;155(4):934-947.

   doi: 10.1016/j.cell.2013.09.053

7. Whyte WA, Orlando DA, Hnisz D, *et al.* Master transcription factors and mediator establish super-enhancers at key cell identity genes. *Cell*. 2013;153(2):307-319.

   doi: 10.1016/j.cell.2013.03.035

8. Chen H, Li C, Peng X, Zhou Z, Weinstein JN, Liang H. A pan-cancer analysis of enhancer expression in nearly 9000 patient samples. *Cell*. 2018;173(2):386-99.e12.

   doi: 10.1016/j.cell.2018.03.027

9. Lovén J, Hoke HA, Lin CY, *et al.* Selective inhibition of tumor oncogenes by disruption of super-enhancers. *Cell*. 2013;153(2):320-334.

   doi: 10.1016/j.cell.2013.03.036

10. Sengupta S, George RE. Super-enhancer-driven transcriptional dependencies in cancer. *Trends Cancer*. 2017;3(4):269-281.

    doi: 10.1016/j.trecan.2017.03.006

11. Yuan J, Jiang YY, Mayakonda A, *et al.* Super-enhancers promote transcriptional dysregulation in nasopharyngeal carcinoma. *Cancer Res*. 2017;77(23):6614-6626.

    doi: 10.1158/0008-5472.can-17-1143

12. Zhang X, Choi PS, Francis JM, *et al.* Identification of focally amplified lineage-specific super-enhancers in human epithelial cancers. *Nat Genet*. 2016;48(2):176-182.

    doi: 10.1038/ng.3470

13. Gryder BE, Yohe ME, Chou HC, *et al.* PAX3-FOXO1 establishes myogenic super enhancers and confers bet bromodomain vulnerability. *Cancer Disco.* 2017;7:8848-99.

    doi: 10.1158/2159-8290.Cd-16-1297

14. Tan M, Pan Q, Gong H, *et al.* Super-enhancer-associated SNHG15 cooperating with FOSL1 contributes to bladder cancer progression through the WNT pathway. *Pharmacol Res*. 2023;197:106940.

    doi: 10.1016/j.phrs.2023.106940

15. Wang X, Zhang R, Wu S, *et al.* Super-enhancer LncRNA LINC00162 promotes progression of bladder cancer. *iScience*. 2020;23(12):10185.

    doi: 10.1016/j.isci.2020.101857

16. Wu Q, Li P, Tao X, Lin N, Mao B, Xie X. A novel super-enhancer-related risk model for predicting prognosis and guiding personalized treatment in hepatocellular carcinoma. *BMC Cancer*. 2024;24(1):1087.

    doi: 10.1186/s12885-024-12874-7

17. Zheng C, Zheng L, Yoo JK, *et al.* Landscape of infiltrating T cells in liver cancer revealed by single-cell sequencing. *Cell*. 2017;169(7):1342-1356.e16.

    doi: 10.1016/j.cell.2017.05.035

18. Chen YP, Yin JH, Li WF, *et al.* Single-cell transcriptomics reveals regulators underlying immune cell diversity and immune subtypes associated with prognosis in

nasopharyngeal carcinoma. *Cell Res*. 2020;30(11):1024-1042.

doi: 10.1038/s41422-020-0374-x

19. Liu Y, Yang X, Gan J, Chen S, Xiao ZX, Cao Y. CB-Dock2: Improved protein-ligand blind docking by integrating cavity detection, docking and homologous template fitting. *Nucleic Acids Res*. 2022;50(W1):W159-W64.

doi: 10.1093/nar/gkac394

20. Huang F, Qi H. MiR-29c-3p/C1QTNF6 restrains the angiogenesis and cell proliferation, migration and invasion in head and neck squamous cell carcinoma. *Mol Biotechnol*. 2023;65(6):913-921.

doi: 10.1007/s12033-022-00591-0.

21. Liu Y, Zhang X, Pang Z, *et al.* Prediction of prognosis and immunotherapy efficacy based on metabolic landscape in lung adenocarcinoma by bulk, single-cell RNA sequencing and Mendelian randomization analyses. *Aging (Albany NY)*. 2024;16(10):8772-8809.

doi: 10.18632/aging.205838

22. Dobruch J, Oszczudłowski M. Bladder cancer: Current challenges and future directions. *Medicina* (*Kaunas*). 2021;57(8):749.

doi: 10.3390/medicina57080749

23. Zhuang HH, Qu Q, Teng XQ, Dai YH, Qu J. Superenhancers as master gene regulators and novel therapeutic targets in brain tumors. *Exp Mol Med*. 2023;55(2):290-303.

doi: 10.1038/s12276-023-00934-0

24. Herranz D, Ambesi-Impiombato A, Palomero T, *et al.* A NOTCH1-driven MYC enhancer promotes T cell development, transformation and acute lymphoblastic leukemia. *Nat Med*. 2014;20(10):1130-1137.

doi: 10.1038/nm.3665

25. Sharma P, Hu-Lieskovan S, Wargo JA, Ribas A. Primary, adaptive and acquired resistance to cancer immunotherapy. *Cell*. 2017;168(4):707-723.

doi: 10.1016/j.cell.2017.01.017

26. Miao D, Margolis CA, Gao W, *et al.* Genomic correlates of response to immune checkpoint therapies in clear cell renal cell carcinoma. *Science*. 2018;359(6377):801-806.

doi: 10.1126/science.aan5951

27. Costa A, Kieffer Y, Scholer-Dahirel A, *et al.* Fibroblast heterogeneity and immunosuppressive environment in human breast cancer. *Cancer Cell*. 2018;33(3):463-79.e10.

doi: 10.1016/j.ccell.2018.01.011

28. Chen X, Song E. Turning foes to friends: Targeting cancer-associated fibroblasts. *Nat Rev Drug Discov*. 2019;18(2):99-115.

doi: 10.1038/s41573-018-0004-1

29. Sahai E, Astsaturov I, Cukierman E, *et al.* A framework for advancing our understanding of cancer-associated fibroblasts. *Nat Rev Cancer*. 2020;20(3):174-186.

doi: 10.1038/s41568-019-0238-1

30. Cai S, Zhang B, Huang C, *et al.* CTRP6 protects against ferroptosis to drive lung cancer progression and metastasis by destabilizing SOCS2 and augmenting the xCT/GPX4 pathway. *Cancer Lett*. 2023;579:216465.

doi: 10.1016/j.canlet.2023.216465

31. Lin CY, Erkek S, Tong Y, *et al.* Active medulloblastoma enhancers reveal subgroup-specific cellular origins. *Nature*. 2016;530(7588):57-62.

doi: 10.1038/nature16546

32. Zhang Z, Zhu H, Wang X, Lin S, Ruan C, Wang Q. A novel basement membrane-related gene signature for prognosis of lung adenocarcinomas. *Comput Biol Med*. 2023;154:106597.

doi: 10.1016/j.compbiomed.2023.106597

33. Binnewies M, Roberts EW, Kersten K, *et al.* Understanding the tumor immune microenvironment (TIME) for effective therapy. *Nat Med*. 2018;24(5):541-550.

doi: 10.1038/s41591-018-0014-x

34. Qu HX, Cui L, Meng XY, *et al.* C1QTNF6 is overexpressed in gastric carcinoma and contributes to the proliferation and migration of gastric carcinoma cells. *Int J Mol Med*. 2019;43(1):621-629.

doi: 10.3892/ijmm.2018.3978

35. Dong X, Hu H, Fang Z, Cui J, Liu F. CTRP6 inhibits PDGF-BB-induced vascular smooth muscle cell proliferation and migration. *Biomed Pharmacother*. 2018;103:844-850.

doi: 10.1016/j.biopha.2018.04.112